

# Low-temperature cycling of isothermal and anhysteretic remanence: microcoercivity and magnetic memory

Adrian R. Muxworthy\*, David J. Dunlop and Özden Özdemir

*Geophysics, Department of Physics, University of Toronto, Toronto, Canada.*

---

## Abstract

This paper reports low-temperature cycling (LTC) through the Verwey transition of anhysteretic remanence (ARM), partial ARMs and partially demagnetised saturation isothermal remanence (SIRM) induced at room temperature in pseudo-single-domain and multidomain (MD) magnetite. The remanences were cooled in zero field to 50 K and then heated back to room temperature. By inducing partial ARMs over different field ranges and by partially alternating field demagnetising SIRMs, it was possible to isolate both low-coercive-force and high-coercive-force fractions of remanence. On cooling through the Verwey transition, a sharp increase in the remanence was observed. The relative size of the jump increased as the high-coercive-force fraction was increasingly isolated. This behaviour is interpreted as being due to both an increase in the single-domain/multidomain threshold size on cooling through the Verwey transition and to the reduction or elimination of closure domains in the low-temperature phase. In addition the memory ratio, i.e., the fraction of remanence remaining after LTC divided by the initial remanence, was found to be higher for the high-coercive-force fraction than the low-coercive-force fraction. In our interpretation, the high-coercivity fraction behaviour is associated with

reversible domain re-organisation effects, whilst the low-coercive force fraction's behaviour is associated with irreversible domain re-organisation and (de-)nucleation processes. Due to the decrease in magnetocrystalline anisotropy on cooling to the Verwey transition, the high-coercive force fraction is likely to be magnetoelastically controlled. Thus, a rock displaying high-coercive force behaviour is likely to carry a palaeomagnetically meaningful remanence with high unblocking temperatures. In addition LTC analysis can be used to identify the domain state dominating the natural remanence in magnetite-bearing rocks.

*Key words:* magnetite, Verwey transition, domain state, coercivity, remanence

---

## 1 Introduction

Zero-field low-temperature cycling (LTC) of magnetite-bearing rocks from room temperature to liquid nitrogen temperature causes varying degrees of partial demagnetisation of remanence depending on domain state [1–8]. The partial demagnetisation is thought to be primarily related to changes in the magnetocrystalline anisotropy, but the exact processes governing LTC behaviour are still unresolved. There is a need for greater understanding if LTC is to become a reliable palaeomagnetic or environmental magnetic technique.

To understand the mechanisms controlling demagnetisation, it is revealing to study the LTC behaviour of various initial remanence states. The direct measurement of remanence during LTC has not been extensive; previous studies

---

\* Now at: Department of Geology & Geophysics, University of Edinburgh, King's Buildings, West Mains Road, Edinburgh, EH9 3JW, UK. email: adrian.muxworthy@ed.ac.uk

have predominantly considered saturation isothermal remanence (SIRM) [1–4,6–8]. It is found that SIRM induced in a multidomain (MD) sample at room temperature gradually decreases on cooling to the magnetocrystalline energy isotropic point  $T_K$  at 130 K and the Verwey transition  $T_V$  at 120–124 K [9,10]. This decrease in remanence has been associated with domain re-ordering effects, i.e., domain wall re-equilibration or domain nucleation, [4,7]. On cooling through  $T_V$ , an increase in magnetisation or “jump” is observed. The size of the jump for SIRM carried by assemblages of crystals is relatively small compared to that of SIRM induced in orientated single crystals  $\sim$  1–4 mm in diameter [6,8]. Below  $T_V$  in the monoclinic/triclinic phase of magnetite, SIRM displays thermally reversible behaviour. On warming through  $T_V$ , the jump is found to be mainly, though not always, reversible. On warming from  $T_K$  to room temperature, SIRM displays irreversible behaviour, with some increase in magnetisation (recovery). The degree of recovery is found to be dependent on internal stress [11], and has been associated with the stiffening of domain walls on heating [7].

There are a limited number of studies of the low-temperature cycling of thermoremanent magnetisation (TRM) [1,7,12], of which by far the most extensive is the paper of Muxworthy & McClelland [7] who measured LTC behaviour of TRM and partial TRMs (pTRM) induced in well characterised synthetic and natural stoichiometric pseudo-single-domain (PSD) and MD magnetites. TRM and pTRM carried by assemblages of magnetite crystals consistently displayed a large jump on cooling through  $T_V$ . The size of the jump was influenced by grain size, the temperature range over which the pTRM was acquired and inducing field intensity, e.g., high-temperature pTRMs induced in small fields in PSD samples displayed larger jumps than pTRMs induced in larger

fields in large MD samples at lower temperatures. The size of the jump was on average larger than that observed for the same samples carrying an SIRM [7]

In addition to experiments, micromagnetic and other numerical models of single sub-micron crystals predict the jump behaviour at  $T_V$  for simulated SIRM, TRM and pTRM structures [5,13]. However, due to the simplifications of the model the size of the simulated jump was larger than that observed for assemblages of small PSD magnetites.

The behaviour at  $T_V$  was explained by a shift in domain state to a more single domain-like (SD) structure and the removal of closure domains in the monoclinic phase [5,7,8]. This was concluded by examining hysteresis data, micromagnetic solutions and by considering the relative anisotropy which indicates the favourability of closure domains [5,8,14]. It was suggested that closure domains play a more important role in reducing the demagnetising energy in small grains than larger grains and in pTRM structures acquired at high-temperatures.

The results of TRM LTC curves have been revealing, but our current knowledge of MD TRM acquisition is incomplete, making it difficult to fully interpret such LTC data. To quantify and improve our understanding of the behaviour of remanence at low temperatures, in this paper LTC curves of partially alternating-field (AF) demagnetised SIRM, anhysteretic remanence (ARM) and partial ARM (pARM) are presented. It is the first time LTC curves for such remanences have been reported. Although these remanences in MD magnetite are not fully understood [15], our knowledge is better than that of TRM as we can more accurately identify which part of the coercivity

spectrum is affected during the induction.

## Sample description

Magnetite samples from two different origins were utilised in this study; three small commercial MD samples  $W(1.7 \mu\text{m})$ ,  $W(7.0 \mu\text{m})$  and  $W(11 \mu\text{m})$ , acquired from Wright Industries, and two MD synthetic samples made by hydrothermal recrystallisation.

The Wright samples were obtained six months before the experimentation and stored in a desiccator. Grain size distributions were found to be log-normal from scanning electron microscope photographs (Table 1). XRD spectra measured shortly after receiving the samples appeared to be those of pure magnetite within experimental limits. However, during the LTC measurements at the Institute for Rock Magnetism, Mössbauer spectra measured using a  $^{57}\text{Co}$  source identified non-stoichiometric magnetite (Figure 1). It is uncertain whether this partial oxidation occurred during the six months of storage or if the samples were initially non-stoichiometric.

Mössbauer parameters were determined by fitting 2 sextets (A and B) using a Lorentzian fitting program (Table 2). The oxidation state of the samples was estimated by considering the ratio of the area of the two sextets ( $F_A$  and  $F_B$ ). For stoichiometric magnetite the ratio  $F_B/F_A$  is experimentally  $\sim 1.9$  [16]. Two possible interpretations are considered; the first is that there are two separate phases within the sample, i.e., a stoichiometric maghemite phase and a stoichiometric magnetite phase. The second interpretation is that the samples are homogeneous cation-deficient magnetite with a formula given

by  $\text{Fe}_{2+2z/3}^{3+}\text{Fe}_{1-z}^{2+}\square_{z/3}\text{O}_4$ ,  $0 \leq z \leq 1$ , where  $\square$  = cation vacancy. In reality it is likely that neither model is correct and the mineralogy is a mixture of both. It is possible to differentiate between two such configurations by measuring Mössbauer spectra in the presence of an external field [16]. However, this facility was not available. The two-phase model is relatively straightforward to determine. The oxidation parameter  $z$  was determined by comparing the  $F_B/F_A$  ratios in Table 2 to the average of the experimental data in Ramdani et al. [17] and Schmidbauer & Keller [18]. The degree of oxidation was found to decrease with grain size. For the two-phase model, the percentage of maghemite was determined to be  $\approx 12\%$  in  $W(1.7\ \mu\text{m})$  and only  $\approx 2.3\%$  in  $W(11\ \mu\text{m})$ . In the cation-deficient model,  $z$  drops from 0.045 for  $W(1.7\ \mu\text{m})$  to 0.009 for  $W(11\ \mu\text{m})$ .

The stoichiometry was checked magnetically by examining both the Curie and Verwey temperatures. The Curie temperatures were determined by measuring thermomagnetic curves on a Princeton Measurements vibrating sample magnetometer (VSM). The Curie temperatures were  $583 \pm 1\ ^\circ\text{C}$ , which is a little above that of stoichiometric magnetite of  $575\text{-}580\ ^\circ\text{C}$  [19].

The Verwey transition was examined by measuring susceptibility using a Lakeshore Cryotronics AC susceptometer (Figure 2). The transition was relatively sharp in  $W(11\ \mu\text{m})$ , indicating near-stoichiometric magnetite, but broader in  $W(1.7\ \mu\text{m})$ . It is uncertain whether this broadening in the smaller grains is due to differences in stoichiometry and/or grain size.

The second set of samples,  $H(39\ \mu\text{m})$  and  $H(108\ \mu\text{m})$ , were produced by the hydrothermal recrystallisation method [20]. The magnetic properties of these samples have been reported several times previously [7,21]. Grain size distri-

butions and magnetic parameters of the samples are summarised in Table 1. XRD analysis and Mössbauer spectroscopy found that the samples were pure magnetite. The samples were dispersed in KBr pellets, and then vacuum sealed in quartz capsules. As the samples were stored in vacuum, oxidation was not expected. However, to check, warming curves for an SIRM at 35 K were measured using a Quantum Design MPMS. A very sharp Verwey transition was observed, indicating stoichiometric magnetite.

Magnetic hysteresis parameters were measured at room temperature for all six samples using the VSM (Table 1). The hydrothermally grown samples have very low values for coercive force ( $H_c$ ) and low saturation remanence ( $M_{rs}$ ) to  $M_s$  ratios, suggesting low dislocation densities. The Wright samples have slightly higher  $H_c$  and  $M_{rs}/M_s$  values, indicating an increased level of internal stress which may be related to the non-stoichiometry. In addition to the hysteresis properties, first-order reversal curve (FORC) diagrams have been measured for these samples at room temperature [21].

## Experimental methods

A series of LTC experiments were made; samples were given either an ARM, pARM or partially demagnetised SIRM, and the behaviour of the remanence was measured during LTC. These experiments were designed to examine how different fractions of the coercivity spectrum behave during LTC.

ARMs and pARMs were induced with a DTech pARM inducer/demagnetiser. The maximum AC field was 200 mT. The effect of applying different biasing DC fields over different field ranges was examined. Partially demagnetised

SIRMs were examined by first inducing an SIRM in a field of 1 T using an ASC pulse magnetiser. The samples were then partially demagnetised using the AF demagnetiser.

Low-temperature behaviour of remanence was measured using an MPMS. Before measuring the LTC curves, the internal field inside the MPMS was reduced to  $\pm 0.5 \mu\text{T}$ . To test the effects of small biasing fields on LTC curves, Muxworthy & McClelland [7] applied fields up to  $\sim 500 \mu\text{T}$  during LTC of SIRM. They found that although the field induced a magnetisation which shifted the LTC curves in the direction of the biasing field, the overall behaviour of the low-temperature thermomagnetic curve was not effected, i.e., the jump feature at  $T_V$  still existed regardless of the bias field direction. They concluded that small biasing fields of the size  $\pm 0.5 \mu\text{T}$  were not the cause of the jump behaviour on cooling through  $T_V$ .

## Results

### *Low-temperature cycling of partially AF demagnetised SIRM*

For three samples,  $W(7.0 \mu\text{m})$ ,  $H(39 \mu\text{m})$  and  $H(108 \mu\text{m})$ , LTC curves were measured for partially AF-demagnetised SIRMs (Figure 3). The general shape of the undemagnetised SIRM LTC curves was in good agreement with previously published data for assemblages of PSD and MD magnetite [2–4,7]. As the peak AF demagnetisation field increases, several features are observed. First, the demagnetisation which occurs on cooling to  $T_K$ , associated with domain wall re-ordering, decreases. Second, a sudden increase or jump occurs on cooling through  $T_V$  for peak AF  $\geq 50 \text{ mT}$ . Third, the memory ratio, i.e., (memory



remanence)/(initial remanence), increases. The width of the Verwey transition was greater in sample  $W(7.0 \mu\text{m})$  than in  $H(39 \mu\text{m})$  and  $H(108 \mu\text{m})$ , most likely because of differences in stoichiometry.

The sharp change in magnetisation at  $T_V$  is characterised by a new parameter, the “Verwey jump” ( $\Delta_{VJ}$ ), which is defined as the size of the increase or decrease in magnetisation across the Verwey transition on cooling normalised by the room temperature magnetisation. Specifically, we calculated  $\Delta_{VJ}$  as the jump in magnetisation over a 10 K interval, starting at  $T_V$  and ending 10 K below  $T_V$ , divided by the initial magnetisation. Because  $T_V$  decreases if magnetite contains impurities or is partially oxidised [9],  $T_V$  should be identified by eye for each individual sample as the temperature at which the magnetisation begins to change sharply. Commonly  $T_V$  is associated with a minimum or a “wild zone” [3] in the temperature range 110-130 K. For all the samples in this study,  $T_V$  was at  $\approx 124$ -125 K. Both positive and negative values for  $\Delta_{VJ}$  have been previously observed [1,6,7].

The absolute values of the jump, i.e.,  $\Delta_{VJ} \times$  the initial remanent magnetisation, increase for  $W(7.0 \mu\text{m})$  and  $H(39 \mu\text{m})$  showing a peak at an alternating field of 50 mT, before decreasing gradually with increasing AF (Figure 4a). For  $H(108 \mu\text{m})$  the absolute jump size decreases with alternating field. In contrast,  $\Delta_{VJ}$  is seen to increase as a function of peak AF for samples  $W(7.0 \mu\text{m})$ ,  $H(39 \mu\text{m})$  and  $H(108 \mu\text{m})$  (Figure 4b). That is, the relative size of the jump increases with peak AF, suggesting that  $\Delta_{VJ}$  is associated with the high-coercivity fraction.

The memory ratio is also seen to increase with peak AF (Figure 4c), supporting the idea that the high-coercivity component of remanence displays reversible

behaviour to LTC [7]. The AF demagnetised memory ratio increases with peak AF for  $W(7.0 \mu\text{m})$ , reaching a value of one at 100 mT.

From the complete data set for each sample, it is possible to construct standard AF demagnetisation curves for both initial remanence and memory (Figure 5). The initial remanence is more easily demagnetised than its memory until some AF level is reached where the two AF demagnetisation curves become identical. Similar contrasts between AF demagnetisation curves of initial remanence and memory have been reported previously [7,22–24].

### *Low-temperature cycling of pARM*

LTC curves were measured for pARM induced in samples  $W(1.7 \mu\text{m})$  and  $H(39 \mu\text{m})$  using a DC field of 200  $\mu\text{T}$  (Figure 6). The maximum AF was always set to 200 mT.  $\Delta_{\text{VJ}}$  and the memory ratios increased with the AF field range over which the pARM was induced for both  $W(1.7 \mu\text{m})$  and  $H(39 \mu\text{m})$  (Figures 6 and 7). For pARM<sub>0</sub><sup>20</sup>, i.e., a pARM induced between AFs of 20-0 mT,  $\Delta_{\text{VJ}}$  for  $H(39 \mu\text{m})$  was observed to be negative. Negative  $\Delta_{\text{VJ}}$  values have been observed before for various types of TRMs induced in large MD magnetites [1,7]. That  $\Delta_{\text{VJ}}$  is a maximum for high AF ranges supports the idea that  $\Delta_{\text{VJ}}$  is related to the high-coercive force fraction.

For sample  $W(1.7 \mu\text{m})$ , the memory ratio for pARM<sub>0</sub><sup>20</sup> is smaller than the ARM memory ratio, i.e., pARM<sub>0</sub><sup>200</sup>. The ratios were 40 % and 92 % respectively, supporting the idea that low-temperature demagnetisation is related to the low-coercivity fraction as suggested by Figures 3 and 4.  $H(39 \mu\text{m})$  displayed different behaviour, and the memory ratios for pARM<sub>0</sub><sup>20</sup> and ARM were

respectively 18 % and 4 %. It is unclear why the memory ratio for ARM was less than any of the pARM memory ratios (Figure 7).

From the pARM data it is possible to determine remanence acquisition distributions. For  $W(1.7 \mu\text{m})$  the peak in the distribution was for pARM<sub>20</sub><sup>50</sup>, whereas  $H(39 \mu\text{m})$  displayed a maximum in the distribution at low-field ranges, i.e., pARM<sub>0</sub><sup>20</sup>. These correspond well with cross-sections of the FORC distribution along the  $H_C$ -axis (x-axis) reported in Muxworthy & Dunlop [21].

### *Effect of ARM acquisition field on LTC behaviour*

In Figure 8, LTC curves for  $W(11 \mu\text{m})$  are shown for ARMs produced with a range of DC fields. As the DC biasing field increases, the shape of the LTC curves evolves, with  $\Delta_{VJ}$  decreasing (Figure 9). For the larger DC fields, ARM LTC curves resembled SIRM LTC curves (Figure 3). The memory ratio also decreases with DC field (Figure 9). This field dependent behaviour is similar to that observed for TRM [7].

ARM and ARM memory acquisition curves were linear with applied field up to 200  $\mu\text{T}$ , in agreement with Muxworthy & McClelland [7] who measured such linear trends for acicular SD magnetite, and hydrothermal and natural MD magnetite.

LTC curves for ARM induced in samples  $W(1.7 \mu\text{m})$  and  $W(7.0 \mu\text{m})$  in a DC field of 200  $\mu\text{T}$  displayed similar behaviour to  $W(11 \mu\text{m})$  (Figure 8), i.e.,  $\Delta_{VJ} = 0$ . The memory ratio gradually decreased with grain size, i.e., 92 %, 47 % and 31 % for samples  $W(1.7 \mu\text{m})$ ,  $W(7.0 \mu\text{m})$  and  $W(11 \mu\text{m})$  respectively. It is uncertain what contribution the differences in stoichiometry made to these

memory ratios.

### *Reversibility of ARM LTC*

To check for reversibility, an ARM (DC field = 200  $\mu$ T) was induced in sample  $W(11 \mu\text{m})$  at room temperature and the remanence gradually cycled between room temperature and increasingly lower temperatures (Figure 10). The induced ARM is seen to partially demagnetise on cooling to temperatures  $> T_V$  and  $T_K$ , e.g., cooling to 150 K is sufficient to demagnetise 22 % of the initial ARM on warming to room temperature. Similar data have been reported for low-temperature cycled SIRM [4,7]. This result strongly supports the theory that domain wall re-organisation during cooling above  $T_K$  is a major contributor to the total low-temperature demagnetisation. On cooling through  $T_V$ , the memory ratio is seen to drop sharply, indicating that significant demagnetisation occurs on cooling through  $T_K$  and  $T_V$ .

## **Discussion**

There are large variations in both the initial remanences and LTC curves shown in this paper. However, there are two clear trends. First, initial remanences associated with higher coercivity fractions display the highest  $\Delta_{VJ}$  values, e.g.,  $\Delta_{VJ}$  is largest for SIRM AF demagnetised to 100 mT (Figure 3) and pARM $_{180}^{200}$  (Figure 6). Secondly, the high coercivity fraction is generally reversible during LTC, i.e., the high-coercivity remanences have the highest memory ratios (Figures 4 and 7). Irreversible behaviour is observed when the lower coercivity fraction of remanence is present.

$\Delta_{VJ}$  displays a grain size dependence (Figures 4 and 7).  $\Delta_{VJ}$  for  $H(39 \mu\text{m})$  and  $H(108 \mu\text{m})$  is greater than  $\Delta_{VJ}$  for  $W(1.7 \mu\text{m})$  for all peak AFs of SIRM. However, as the peak AF increases,  $\Delta_{VJ}$  for  $H(39 \mu\text{m})$  becomes greater than  $\Delta_{VJ}$  for  $H(108 \mu\text{m})$  (Figure 4).  $\Delta_{VJ}$  for all the pARMs is greater for  $H(39 \mu\text{m})$  than  $W(1.7 \mu\text{m})$  except for the pARM<sub>0</sub><sup>20</sup>  $\Delta_{VJ}$ , which is negative for  $H(39 \mu\text{m})$  and zero for  $W(1.7 \mu\text{m})$ .

The memory ratio displays a consistent grain size dependence (Figures 4c and 9). Such grain size dependence of the memory fraction is well documented for other types of remanence [22,23,25]

$\Delta_{VJ}$  decreases strongly with increasing ARM DC field (Figure 9). The memory ratio displays a weaker dependence on ARM DC field. Muxworthy & McClelland [7] observed a similar field dependence of  $\Delta_{VJ}$  for pTRM induced in hydrothermally-grown MD magnetites for fields between 100  $\mu\text{T}$  and 5 mT. They related the LTC behaviour of the high-field remanence to a shift in domain structure to a more SIRM-like structure. SIRM structures generally have smaller  $\Delta_{VJ}$  values [5,7].  $\Delta_{VJ}$  for an initial SIRM was zero for Wright sample  $W(1.7 \mu\text{m})$ , although for some samples  $\Delta_{VJ}$  SIRM  $> 0$ , e.g.,  $H(108 \mu\text{m})$  (Figure 4b). Drawing together the results in this study, the effect of decreasing the ARM DC field is to increase the relative size of the high-coercivity fraction of remanence.

### *Origin of $\Delta_{VJ}$*

In previous papers, simple mutually compatible models were developed to explain positive  $\Delta_{VJ}$  behaviour [5–8].  $\Delta_{VJ}$  was attributed to both a shift to

a more SD-like domain state and the removal of closure-like domains in the monoclinic phase [5,7,8].

The shift in domain state is related to the large increase in the magnetocrystalline anisotropy on cooling through  $T_V$ , causing the SD/MD threshold size to increase [5,8]. On cooling through  $T_V$  the domain structure tries to denucleate walls, or at least re-equilibrate walls to reduce the total energy. This will on average increase the measured magnetisation of a sample. Generally denucleation of domain walls is thought to be irreversible, whilst wall re-equilibration is reversible.

That the isolated high-coercive-force fraction of remanence displays reversible behaviour at  $T_V$  suggests that its behaviour is controlled by domain wall re-equilibration processes (e.g., Figures 3 and 6).

The contribution of removing closure domains to  $\Delta_{VJ}$  is more debatable, especially for small PSD grains. Closure domains have been clearly observed in large MD magnetite [26]. In small PSD magnetite such features are generally not observed [27,28]. However, grain-edge features which reduce the magnetic flux leakage in PSD magnetite are predicted to exist and to be difficult to observe experimentally [29]. On simulated cooling through the Verwey transition, the removal of such features was the main contributor to  $\Delta_{VJ}$  [5].

The high-coercive-force fraction of remanence is more likely than the low-coercive-force fraction to be associated with domain configurations where domain walls are pinned far from their equilibrium positions. To reduce the energy of these states in the cubic phase, closure domains are likely to form. The removal of such closure domains will result in an increase in  $\Delta_{VJ}$ . Experimentally,  $\Delta_{VJ}$  becomes relatively larger as the higher coercive fraction

becomes increasingly isolated (Figures 4 and 7).

The relative increase in  $\Delta_{VJ}$  from both of these effects will be greater for small grains, e.g., reducing a domain structure from two domains to a SD will lead to a bigger increase in  $\Delta_{VJ}$  than decreasing from, say, 20 domains to 18, and the importance of closure domains is also greater for domain structures with only a few domains. In contrast, the results in this paper show that  $\Delta_{VJ}$  increases with grain size (Figures 4 and 7). This discrepancy may be due to the very different microcoercivity distributions of the Wright and hydrothermal samples; the influence of microcoercivity may mask the expected grain size trend. Özdemir et al.[8] found a similar grain size relationship for SIRMs, whereas Muxworthy & McClelland [7] found that  $\Delta_{VJ}$  for TRM increased as the grain size was decreased.

In addition to these two mechanisms, twin domain (TD) structures are thought to be important to the low-temperature magnetic behaviour due to the high magnetocrystalline anisotropy [6–8]. However, it is difficult to assess their importance as certain key facts are unknown. Firstly, there may or may not be TD boundaries as there is a single-TD to multi-TD critical size [30,31]. The critical size depends on the boundary conditions of each grain, and it is not possible to roughly estimate the critical size as this is a highly non-linear calculation [*pers. comm.* A. Jacobs, 2002]. Secondly, the interaction of remanence structures with TDs is unknown. Either the twin or the magnetic domains could dominate the remanence behaviour depending on whether the strain or magnetic energy dominates [*pers. comm.* A. Jacobs, 2002]. In addition, it is possible due to the symmetry considerations, for certain orientations of TD and magnetic domain walls to re-adjust independently [*pers. comm.* C. Medrano, 1999].

High memory ratios reflect reversible behaviour through the entire LTC curve, including on cooling through  $T_V$  (Figures 3, 6 and 8). Irreversible behaviour is thought to be due to denucleation of domain walls, both on cooling from room temperature to  $T_K$  due to the decrease in the magnetocrystalline anisotropy (Figure 10), and on cooling to below  $T_V$ . High memory ratios were found to be related to high coercivity remanences (Figure 4 and 7). This is in agreement with AF demagnetisation curves of both initial and memory remanence (Figure 5, [7,22,23]). These high-coercivity remanences are more likely to be stress controlled, and hence relatively unaffected by changes in the magnetocrystalline anisotropy. When palaeomagnetic remanences are thermally demagnetised, a magnetoelastically controlled remanence decays much less rapidly than a magnetocrystalline controlled one. Thus a high memory ratio, implying magnetoelastic control, is likely to be an indicator of a palaeomagnetically meaningful remanence with high unblocking temperatures.

## **Conclusions**

This study clearly demonstrates that LTC behaviour is influenced by the coercive force distribution of the remanence. It is shown that key features such as  $\Delta_{VJ}$  and high memory ratios are associated with the highest coercivity fraction of remanence. Some of the LTC behaviour can be explained by the application of previously reported theories [5–8]

The identification of high memory ratios or a significant  $\Delta_{VJ}$  peak for a natural remanent magnetisation (NRM) would indicate that the remanence was



dominated by a magnetoelastically controlled high coercivity signal, and that the sample is suitable for palaeomagnetic investigations. The measurement of memory ratio does not require low-temperature measurements of magnetisation. It is recommended that LTC be used as a pre-selection technique in palaeomagnetic studies, and if applied judiciously it could be used as a cleaning technique [32].

In addition LTC analysis can be used to identify the domain state dominating the NRM signal in magnetite bearing rocks; high memory ratios and large jumps at the Verwey transition indicate a high-coercive force MD remanence, high memory ratios and small jumps at the Verwey transition suggest a SD remanence, whilst low-memory ratios indicate a low-coercive force MD remanence.

## **Acknowledgements**

We benefited from fruitful discussions with Yongjae Yu and Allan Jacobs. Mike Jackson and an anonymous reviewer made constructive comments. We thank Wright Industries for providing the samples. Fred Neub of the Materials Engineering Dept., University of Toronto, helped with the SEM work. The magnetic experiments were made at the Institute for Rock Magnetism, University of Minnesota, which is funded by the National Science Foundation, the W. M.Keck Foundation and the University of Minnesota. We thank Mike Jackson, Peat Sølheid and Jim Marvin for help with the measurements. This research has been supported by the Natural Sciences and Engineering Research Council of Canada through grant A7709 to D.J.D.

## References

- [1] M. Ozima, M. Ozima, S.-T. Akimoto, Low-temperature characterisation of remanent magnetisation of magnetite - self-reversal and recovery phenomena, *J. Geomag. & Geoelec.* 16 (1964) 165–177.
- [2] K. Kobayashi, M. Fuller, Stable remanence and memory of multidomain materials with special reference to magnetite, *Phil. Mag.* 18 (1968) 601–624.
- [3] S. L. Halgedahl, R. D. Jarrard, Low temperature behaviour of single domain through multidomain magnetite, *Earth Planet. Sci. Lett.* 130 (1995) 127–139.
- [4] J. P. Hodych, R. I. Mackay, G. M. English, Low-temperature demagnetization of saturation remanence in magnetite-bearing dolerites of high coercivity, *Geophys. J. Int.* 132 (2) (1998) 401–411.
- [5] A. R. Muxworthy, W. Williams, Micromagnetic models of pseudo-single domain grains of magnetite near the Verwey transition, *J. Geophys. Res.* 104 (1999) 9203–9218.
- [6] Ö. Özdemir, D. J. Dunlop, Low-temperature properties of a single crystal of magnetite orientated along principal magnetic axes, *Earth Planet. Sci. Lett.* 165 (1999) 229–239.
- [7] A. R. Muxworthy, E. McClelland, The causes of low-temperature demagnetisation of remanence in multidomain magnetite, *Geophys. J. Int.* 140 (2000) 115–131.
- [8] Ö. Özdemir, D. J. Dunlop, B. M. Moskowitz, Changes in remanence, coercivity and domain state at low temperature in magnetite, *Earth Planet. Sci. Lett.* 194 (2002) 343–358.
- [9] A. R. Muxworthy, E. McClelland, Review of the low-temperature magnetic

- properties of magnetite from a rock magnetic perspective, *Geophys. J. Int.* 140 (2000) 101–114.
- [10] R. J. Harrison, Magnetic transitions in minerals, in: S. A. T. Redfern, M. A. Carpenter (Eds.), *Reviews in Mineralogy and Geochemistry Volume 39 - Transformation processes in minerals*, Mineralogical Society of America, Washington D. C., 2000, pp. 175–202.
- [11] J. King, W. Williams, Low-temperature properties of magnetite, *J. Geophys. Res.* 105 (B7) (2000) 16427–16436.
- [12] R. L. Hartstra, TRM, ARM and Isr of two natural magnetites of MD and PSD grain size, *Geophys. J. R. Astron. Soc.* 73 (1983) 719–737.
- [13] B. Carter-Stiglitz, M. Jackson, B. M. Moskowitz, Low-temperature remanence in stable single domain magnetite, *Geophys. Res. Lett.* 10.1029/2001GL014197 (2002) 437–450.
- [14] A. Hubert, R. Schäfer, *Magnetic Domains*, Springer Verlag, Berlin, 1998.
- [15] Y. Yu, D. J. Dunlop, Ö. Özdemir, Partial anhysteretic remanent magnetization in magnetite 1. Additivity, *J. Geophys. Res.* in press.
- [16] R. E. Vandenberghe, C. A. Barrero, G. M. Da Costa, E. Van San, E. De Grave, Mössbauer characterization of iron oxides and (oxy)hydroxides: the present state of the art, *Hyperfine Interactions* 126 (2000) 247–259.
- [17] A. Ramdani, J. Steinmetz, C. Gleitzer, J. M. Coey, J. M. D. Friedt, Perturbation de l'échange électronique rapide par les lacunes cationiques dans  $\text{Fe}_{3-x}\text{O}_4$  ( $x \leq 0.09$ ), *J. Phys. Chem. Solids.* 48 (1987) 217–228.
- [18] E. Schmidbauer, R. Keller, Magnetic hysteresis properties,  $^{57}\text{Fe}$  Mössbauer spectra and structural data of spherical 250 nm particles of solid solutions  $\text{Fe}_3\text{O}_4$ - $\gamma$ - $\text{Fe}_2\text{O}_3$ , *J. Magn. Mater.* submitted.

- [19] D. J. Dunlop, Ö. Özdemir, *Rock Magnetism: Fundamentals and Frontiers*, Cambridge University Press, 1997.
- [20] F. Heider, L. T. Bryndzia, Hydrothermal growth of magnetite crystals (1  $\mu\text{m}$  to 1 mm), *J. Crystal Growth* 84 (1987) 50–56.
- [21] A. R. Muxworthy, D. J. Dunlop, First-order reversal curve (FORC) diagrams for pseudo-single-domain magnetites at high temperature, *Earth Planet. Sci. Lett.* 203 (2002) 369–382.
- [22] D. J. Dunlop, K. S. Argyle, Separating multidomain and single-domain-like remanences in pseudo-single-domain magnetites (215–540 nm) by low-temperature demagnetisation, *J. Geophys. Res.* 96 (B2) (1991) 2007–2017.
- [23] E. McClelland, V. P. Shcherbakov, Metastability of domain state in MD magnetite: consequences for remanence acquisition, *J. Geophys. Res.* 100 (B3) (1995) 3841–3857.
- [24] Ö. Özdemir, D. J. Dunlop, Single-domain-like behavior in a 3-mm natural single crystal of magnetite, *J. Geophys. Res.* 103 (B2) (1998) 2549–2562.
- [25] F. Heider, D. J. Dunlop, H. C. Soffel, Low temperature and alternating field demagnetisation of saturation remanence and thermoremanence in magnetite grains (0.037  $\mu\text{m}$  to 5 mm), *J. Geophys. Res.* 97 (B6) (1992) 9371–9381.
- [26] Ö. Özdemir, S. Xu, D. J. Dunlop, Closure domains in magnetite, *J. Geophys. Res.* 100 (B2) (1995) 2193–2209.
- [27] C. E. Geiß F. Heider, H. C. Soffel, Magnetic domain observations on magnetite and titanomaghemite grains (0.5–10  $\mu\text{m}$ ), *Geophys. J. Int.* 124 (1996) 75–88.
- [28] T. G. Pokhil, B. M. Moskowitz, Magnetic domains and domain walls in pseudo-single-domain magnetite studied with magnetic force microscopy, *J. Geophys. Res.* 102 (B10) (1997) 22681–22694.

- [29] W. Williams, T. M. Wright, High resolution micromagnetic models of fine grains of magnetite, *J. Geophys. Res.* B12 (1998) 30537–30550.
- [30] E. K. H. Salje, Ferroelasticity, *Cont. Physics* 41 (2000) 79–91.
- [31] W. Cao, C. A. Randall, Grain size and domain size relations in bulk ceramic ferroelectric materials, *J. Phys. Chem. Solids.* 57 (10) (1996) 1499–1505.
- [32] M. Ozima, M. Ozima, T. Nagata, Low-temperature treatment as an effective means of “magnetic cleaning” of natural remanent magnetisation., *J. Geomag. & Geoelec.* 16 (1964) 37–41.

Table 1

Summary of the grain-size distributions and room-temperature hysteresis parameters for the samples in this study. The Wright samples had lognormal distributions. These were transformed into  $\log_{10}$  space before the mean and standard deviation were calculated. The hydrothermally produced samples displayed a more Gaussian size distribution.  $\sigma$  is the standard deviation of the normal distribution in either case, but  $\sigma$  given in the table for the Wright samples is not symmetric about the mean on a linear scale. The aspect ratio (AR) is the ratio of the long axis over the short axis. No aspect ratio was measured for the hydrothermally produced samples as the grains were nearly all symmetrical. The hysteresis parameters  $H_c$ ,  $H_{cr}$  and  $M_{rs}/M_s$  are shown.

sample	size ( $\mu$ m)		Mean	$H_c$	$H_{cr}$	$M_{rs}/M_s$
	mean	$\sigma$	AR	(mT)	(mT)	
$W(1.7 \mu\text{m})$	1.7 <sup>a</sup>	0.2 <sup>a</sup>	1.4	16.1	39.1	0.149
$W(7.0 \mu\text{m})$	7 <sup>a</sup>	3 <sup>a</sup>	1.0	6.2	24.9	0.065
$W(11 \mu\text{m})$	11 <sup>a</sup>	3 <sup>a</sup>	1.8	4.6	20.4	0.044
$H(39 \mu\text{m})$	39	9	...	1.2	24.7	0.010
$H(108 \mu\text{m})$	108	31	...	0.94	18.2	0.002

<sup>a</sup> converted from  $\log_{10}$  space

Table 2

Mössbauer parameters of two sextets (A and B) for all three Wright samples. Two of the spectra are shown in Figure 1 ( $W(1.7 \mu\text{m})$  and  $W(11 \mu\text{m})$ ). IS = isomer shift (with reference to metallic iron); QS= quadrupole splitting;  $B_{hf}$  = magnetic hyperfine field;  $F_B/F_A$  is the ratio of the area of sextets A and B.  $F_B/F_A$  is calculated assuming  $[\text{Fe}_B^{2+}][\text{Fe}_A^{3+}\text{Fe}_B^{3+}]$ . The two-phase model calculation is made assuming two separate stoichiometric phases, magnetite and maghemite. The estimate for  $z$  was made by comparing  $F_B/F_A$  ratios to those in the literature [17,18].

sample	$B_{hf}$ (T)		QS ( $\text{mms}^{-1}$ )		IS ( $\text{mms}^{-1}$ )		$F_B/F_A$	Two phase	
	A	B	A	B	A	B		% $\gamma\text{-Fe}_2\text{O}_3$	$z$
$W(1.7 \mu\text{m})$	49.4	46.1	-0.02	-0.02	0.28	0.66	1.67	12	0.045
$W(7.0 \mu\text{m})$	49.4	46.2	-0.02	$\sim 0$	0.28	0.67	1.71	10	0.039
$W(11 \mu\text{m})$	49.5	46.1	$\sim 0$	$\sim 0$	0.29	0.67	1.86	2.3	0.009

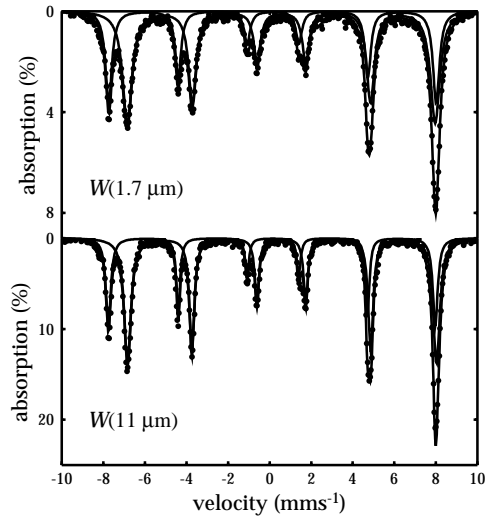


Fig. 1. Room-temperature Mössbauer absorption spectra for samples  $W(1.7 \mu\text{m})$  and  $W(11 \mu\text{m})$ . Two Lorentzian sextets have been fitted to each spectrum.  $W(11 \mu\text{m})$  is nearly stoichiometric magnetite, whereas  $W(1.7 \mu\text{m})$  is slightly non-stoichiometric. The difference between the two spectra is most clearly seen by comparing the peaks on the extreme left. The difference in absorption percentages is simply due to differences in sample mass.



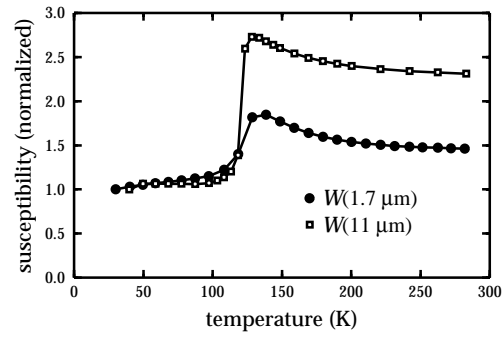


Fig. 2. Low-temperature susceptibility curves for samples  $W(1.7 \mu\text{m})$  and  $W(11 \mu\text{m})$ . The susceptibility was measured during warming for two frequencies; 400 Hz and 4000 Hz. No frequency dependence was observed. Only the 400 Hz data are shown. The samples were cooled in zero field.

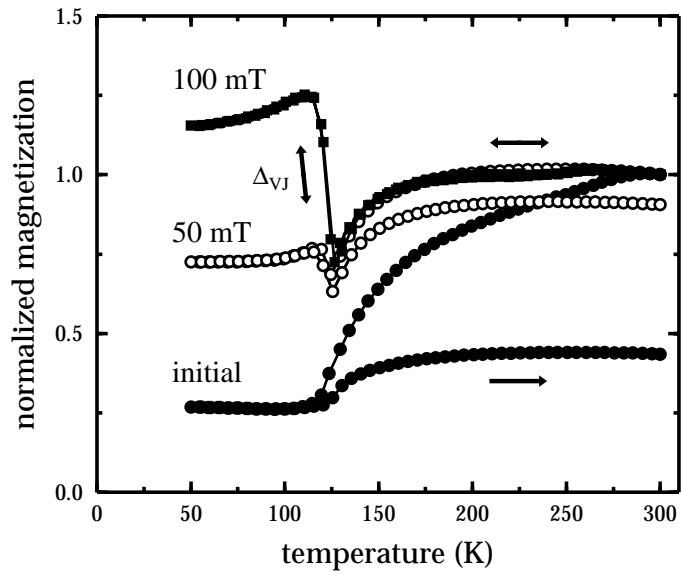


Fig. 3. LTC curves for sample  $W(7.0 \mu\text{m})$  carrying an SIRM, an SIRM AF demagnetised to a maximum field of 50 mT and an SIRM AF demagnetised to 100 mT. The parameter  $\Delta_{vJ}$  is depicted.

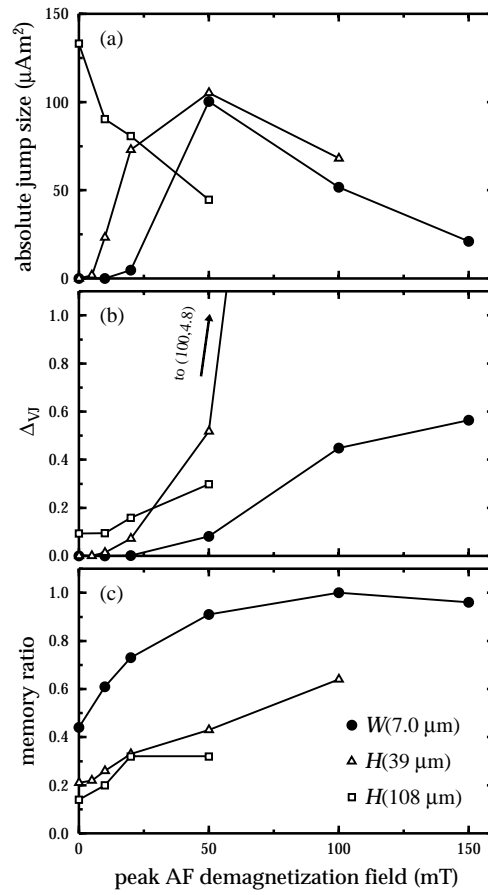


Fig. 4. The absolute jump size (a),  $\Delta V_J$  (b) and the memory ratio (c) versus the peak AF demagnetisation field for samples  $W(7.0 \mu\text{m})$ ,  $H(39 \mu\text{m})$  and  $H(108 \mu\text{m})$  induced initially with an SIRM. The relative absolute values for the jump size between the three samples reflect the relative amount of material in each sample. The maximum AF demagnetisation field for  $H(108 \mu\text{m})$  was 50 mT.

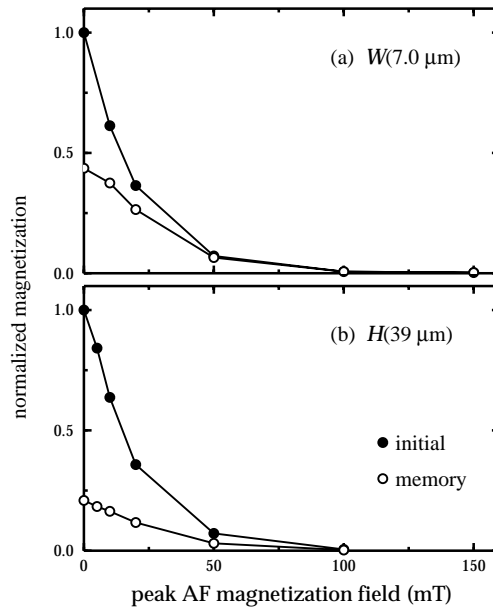


Fig. 5. Simulated AF demagnetisation curves of initial SIRM and SIRM memory for samples a)  $W(7.0 \mu\text{m})$  and b)  $H(39 \mu\text{m})$ . Before each AF demagnetisation step a new SIRM was produced.  $H(108 \mu\text{m})$  displayed similar behaviour to  $H(39 \mu\text{m})$ .

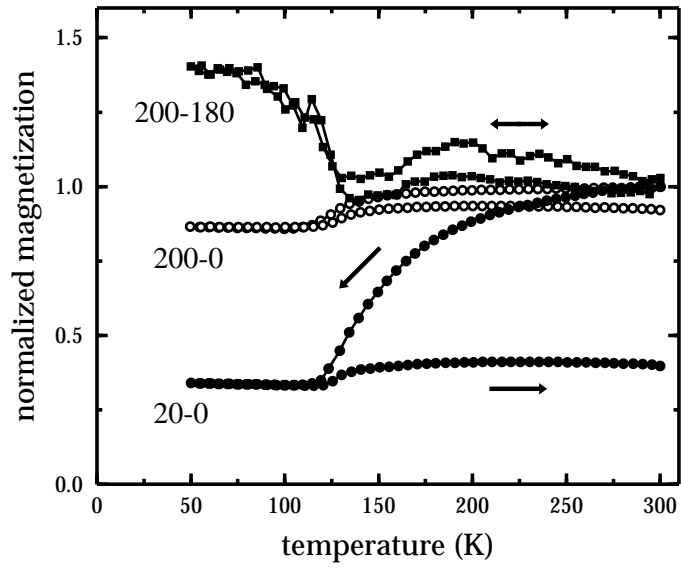


Fig. 6. LTC curves for  $W(1.7 \mu\text{m})$  with pARMs induced over three different ranges;  $\text{pARM}_0^{200}$  (= ARM in other diagrams),  $\text{pARM}_{180}^{200}$  and  $\text{pARM}_0^{20}$ . The peak AF during pARM acquisition was 200 mT, and the DC field was set to  $200 \mu\text{T}$ .

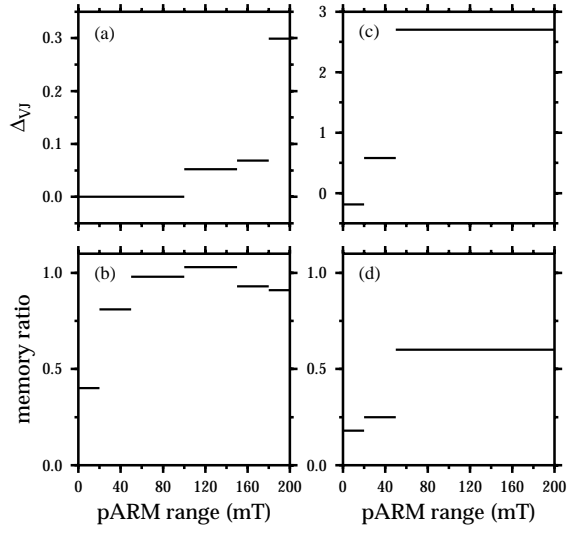


Fig. 7.  $\Delta_{VJ}$  and the memory ratio versus pARM inducing field range for different pARMs in samples  $W(1.7 \mu\text{m})$  (a and b) and  $H(39 \mu\text{m})$  (c and d).  $W(1.7 \mu\text{m})$  had six pARMs induced over the 200 mT range, whilst  $H(39 \mu\text{m})$  had three. The corresponding  $\Delta_{VJ}$  values and memory ratios for a complete ARM were 0 % and 92 % for  $W(1.7 \mu\text{m})$  and 35 % and 4 % for  $H(39 \mu\text{m})$ .

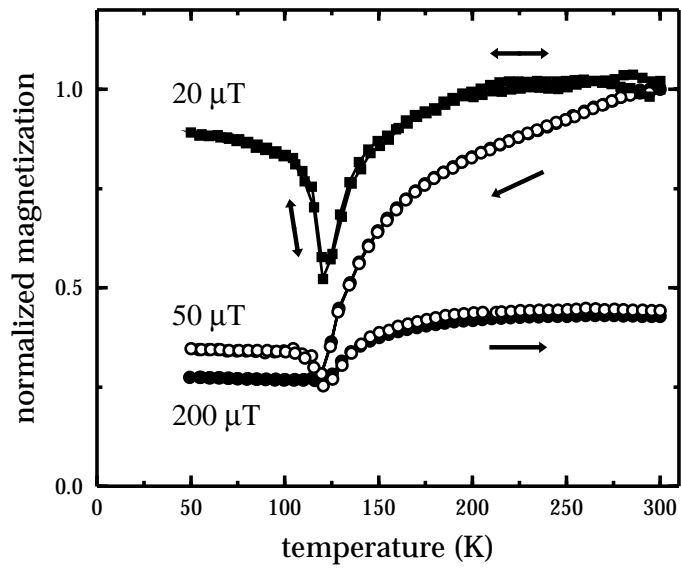


Fig. 8. LTC curves for  $W(11 \mu\text{m})$  with ARMs induced in three different DC fields (20, 50 and 200  $\mu\text{T}$ ). The peak AF during ARM acquisition was 200 mT. The cooling curves for the 50  $\mu\text{T}$  and 200  $\mu\text{T}$  remanences overlap each other.

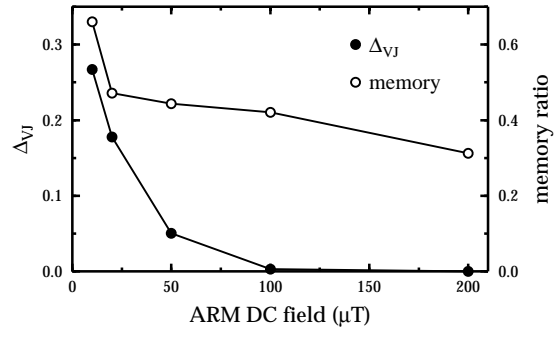


Fig. 9.  $\Delta_{VJ}$  and the memory ratio versus ARM DC acquisition field for sample  $W(11 \mu\text{m})$ .  $\Delta_{VJ}$  was zero for high fields. The peak AF during ARM acquisition was 200 mT.



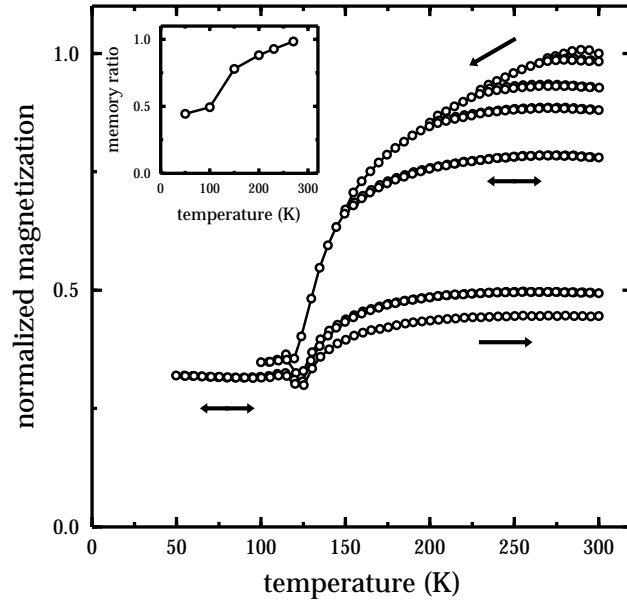


Fig. 10. Low-temperature cycling curves for  $W$  ( $11 \mu\text{m}$ ) induced with an initial ARM (DC field =  $200 \mu\text{T}$ ). The sample was cycled from room temperature to a series of gradually decreasing temperatures. The inset shows the memory ratio as a function of minimum temperature reached after each LTC cycle.